

ECCD Experiments in Heliotron J, TJ-II, CHS, and LHD

Kazunobu NAGASAKI¹⁾, Gen MOTOJIMA²⁾, Angela C. FERNÁNDEZ³⁾, Álvaro A. CAPPA³⁾, Jose Maria FONTDECABA³⁾, Yoshio YOSHIMURA⁴⁾, Takashi NOTAKE⁴⁾, Shin KUBO⁴⁾, Takashi SHIMOZUMA⁴⁾, Hiroe IGAMI⁴⁾, Katsumi IDA⁴⁾, Mikio YOSHINUMA⁴⁾, Takashi KOBUCHI⁴⁾, Heliotron J Team^{1,2)}, TJ-II Team³⁾, CHS Team⁴⁾ and LHD Team⁴⁾

¹⁾*Institute of Advanced Energy, Kyoto University, Uji 611-0011, Japan*

²⁾*Graduate School of Energy Science, Kyoto University, Uji 611-0011, Japan*

³⁾*Laboratorio Nacional de Fusio'n, EURATOM-CIEMAT, Madrid 28040, Spain*

⁴⁾*National Institute for Fusion Science, Toki 509-5292, Japan*

(Received 15 November 2007 / Accepted 5 February 2008)

Electron cyclotron current drive (ECCD) experiments were conducted in the stellarator/heliotron (S/H) devices, such as Heliotron J, TJ-II, CHS, and LHD. Experimental results show that ECCD can be controlled by the power injection angle, absorption position and magnetic field structure. The current drive efficiencies are similar, $\gamma = n_e I_{ECR} / P_{EC} = 8 - 16 \times 10^{16}$ A/Wm², $\zeta = 32.7 n_e I_{ECR} / P_{WT_e} = 0.03 - 0.05$, when the magnetic field ripple ratio is $0.93 < B_{min} / B_{max} < 1.0$. The reversal of driven current direction is observed depending on the magnetic field ripple structure, indicating that the amplitude and direction of EC current is determined by the balance between the Fisch-Boozer effect and the Ohkawa effect, and that the Ohkawa effect is stronger in S/H devices compared with tokamaks. Control of net toroidal current by using ECCD is demonstrated; a net zero current state is attained by cancelling the bootstrap current.

© 2008 The Japan Society of Plasma Science and Nuclear Fusion Research

Keywords: electron cyclotron current drive, stellarator, heliotron, Heliotron J, TJ-II, CHS, LHD, current drive efficiency, Fisch-Boozer effect, Ohkawa effect

DOI: 10.1585/pfr.3.S1008

1. Introduction

Non-inductive current has an important role in realization of high-performance plasmas and sustainment of steady-state plasmas in toroidal fusion devices. In stellarator/heliotron (S/H) systems, no Ohmic current is required for equilibrium since the confinement magnetic field is generated by external coils. However, it is known that finite plasma pressure drives the bootstrap current in S/H systems similar to tokamaks, which modifies the rotational transform profile, thus affecting the equilibrium and stability. For example, the bootstrap current increases the rotational transform in LHD, moving the rational surface of $\iota/2\pi = 1$ to a low-shear region, thus degrading the confinement due to formation of magnetic islands [1].

Electron cyclotron current drive (ECCD) is recognized as a useful scheme for stabilizing MHD instabilities and analyzing heat and particle transport [2, 3]. For example, in large tokamaks such as JT-60U, the neoclassical tearing mode has been stabilized by localized ECCD, leading to improvement of normalized beta [4]. In S/H systems, on the other hand, the ECCD is expected to avoid a dangerous rational surface by cancelling the bootstrap current, particularly in low-shear S/H devices. From the viewpoint of diagnostics, on the other hand, the S/H systems have the advantage of precise measurement of the EC

current. Estimation of EC current is not so simple in tokamaks since a large amount of Ohmic current flows, and the effects of toroidal electric field and plasma resistivity have to be taken into account. In S/H systems, we are able to measure the EC current with an accuracy of the order of less than 1 kA using a conventional Rogowski coil because no Ohmic current flows.

A systematic research on ECCD in S/H systems was performed experimentally in W7-AS for the first time [5, 6]. Several results, such as the dependence on injection angle and electron density, and the effect of trapped particles, were discussed. Recently, international collaboration research on ECCD has been conducted in Heliotron J (Kyoto Univ.) [7], TJ-II (CIEMAT) [8], CHS (NIFS) [9, 10], and LHD (NIFS) [11] in order to understand ECCD physics and to investigate the applicability of ECCD to the control of plasma equilibrium and stability. This paper summarizes these recent experimental results on ECCD. Comparison of experimental results from these four devices will give us a common understanding of current drive physics.

This paper is organized as follows. The experimental setup, including the ECH/ECCD system, is described in Sec. 2. The experimental results, especially the dependence on injection angle, electron density, and magnetic field structure, are discussed in Sec. 3. The trapped par-

author's e-mail: nagasaki@iae.kyoto-u.ac.jp

ticle effect generated by the magnetic field ripple, which strongly affects the current drive efficiency, is also discussed. A summary is given in Sec. 4.

2. Experimental Setup

Heliotron J, TJ-II, CHS, and LHD are S/H fusion devices with the following device parameters: major radius, $R = 1.2$ m, minor radius, $a = 0.1$ – 0.2 m, magnetic field, $B = 1.5$ T (Heliotron J), $R = 1.5$ m, $a = 0.1$ – 0.2 m, $B = 1.0$ T (TJ-II), $R = 1.0$ m, $a = 0.2$ m, $B = 1.9$ T (CHS), and $R = 3.75$ m, $a = 0.6$ m, and $B = 2.8$ T (LHD). The ranges of plasma parameters are $n_e = 0.2$ – 1.5×10^{19} m $^{-3}$, $T_e = 0.3$ – 2 keV and $T_i = 0.1$ – 2 keV. The plasmas are produced and heated only by ECH, and the upper density limit is determined by second-harmonic X-mode cut-off, $n_e^c = 1.75 \times 10^{19}$ m $^{-3}$ for 53.2 GHz (TJ-II and CHS), $n_e^c = 3.0 \times 10^{19}$ m $^{-3}$ for 70 GHz (Heliotron J), $n_e^c = 4.4 \times 10^{19}$ m $^{-3}$ for 84 GHz (LHD) and $n_e^c = 17.5 \times 10^{19}$ m $^{-3}$ for 168 GHz (LHD).

The magnetic field structure of each device is different since the field spectra are different. Figure 1 illustrates the magnetic field profiles along the magnetic axis. Heliotron J has the capability of controlling the coil current independently, making it possible to change the magnetic ripple structure at the launching position. The structure of the magnetic field exists from a local maximum (ripple top structure) to a local minimum (ripple bottom structure) at the ECH power deposition. In TJ-II, the EC power is injected near the local minimum position. In CHS and LHD, the magnetic field ripple is small along the magnetic axis at the magnetic axis location of $R = 0.95$ m and $R = 3.75$ m, respectively, and the ripple structure appears when the magnetic axis is shifted by vertical coils.

The ECH/ECCD system is routinely used for plasma production and heating in S/H systems. Since the S/H system has a 3-D magnetic field structure, a wide injection angle range and precise polarization control are required to change the absorption profile and parallel refractive index. Recent progress in high-power millimeter-wave technology enables a focused Gaussian beam injection system with well-controlled injection angle and polarization. Table 1 shows the main features of the ECH/ECCD systems in Heliotron J, TJ-II, CHS, and LHD (see references for details). The focused Gaussian beam is injected with a wide range of both toroidal and poloidal injection angles using a steering mirror, which enables us to achieve an adequate oblique launch angle for a large refractive index. In TJ-II, two 53.2-GHz ECH/ECCD systems are used; a steering mirror is installed in each injection system. The injection position is symmetric with respect to the toroidal angle, so that the EC current can be controlled by scanning the injection angle with different $N_{||}$. In CHS, the EC beam is injected from the top of the torus, and the refractive index is 0.16 in vacuum at the magnetic axis of $R = 0.95$ m for the toroidal angle of 7 deg. In LHD, the toroidal angle is 8.3 deg at the vertical port (1.5L port) and 9.9 deg at the

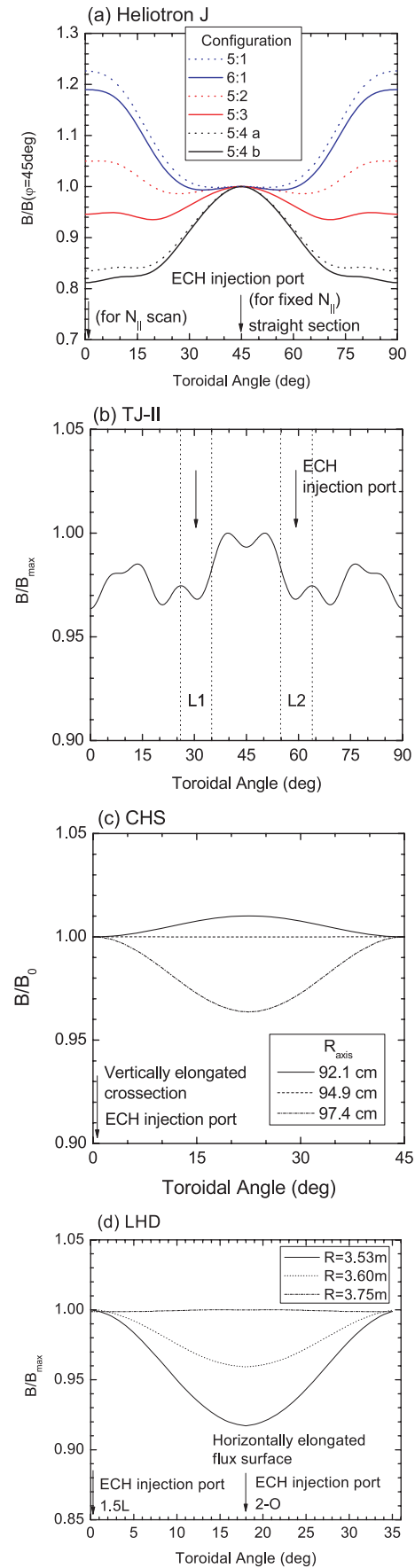


Fig. 1 Magnetic field profile along magnetic axis in (a) Heliotron J, (b) TJ-II, (c) CHS, and (d) LHD.

Table 1 Heating systems for ECCD experiment in Heliotron J, TJ-II, CHS, and LHD.

	Heliotron J	TJ-II	CHS	LHD
Frequency	70 GHz	53.2 GHz	53.2 GHz	84 GHz
Maximum injection power	0.4 MW	2×0.3 MW	0.3 MW	1.3 MW
Maximum pulse length	0.2 sec	0.5 sec	0.1 sec	3 sec
Injection mode	Focused/nonfocused Gaussian	Focused Gaussian	Focused Gaussian	Focused Gaussian
Injection angle	Controllable/Fixed	Controllable	Controllable	Controllable
Polarization	Controllable	Controllable	Controllable	Controllable
Injection mode	2nd X	2nd X	2nd X	1st O/2nd X
Reference	[12]	[13]	[14]	[15]

horizontal port for co-injection; for counter-injection it is -5.9 deg at the vertical port -9.9 deg at the horizontal port.

3. Experimental Results

Plasmas are produced and heated by the second-harmonic X-mode ECH. A rough estimation of development time of total toroidal current is given by L_p/R_p , where L_p and R_p are plasma inductance and resistance, respectively. L_p/R_p is estimated from 0.1 to a few seconds by assuming neoclassical conductivity. The measured toroidal current is continually increased during discharge at low densities so that the current is underestimated in the low-density regime. A finite current may modify the rotational transform, thus affecting global confinement. However, neither strong confinement degradation nor MHD instabilities were observed in the experiment reported here. Details of ECCD experiments in each device are described in Refs. [7–11].

As predicted from the ECCD theory, the amplitude and driven direction depends on the parallel refractive index, N_{\parallel} . Figure 2 shows the dependence of the toroidal angle on the EC injection angle. It can be seen that I_p increases with increasing N_{\parallel} and saturates at a certain N_{\parallel} . ECCD is one of the main contributors to the total current since the bootstrap current is small because of the low pressure at $n_e = 0.5 \times 10^{19} \text{ m}^{-3}$. The flow direction is the one expected from the Fisch-Boozer effect opposite to N_{\parallel} [16]. The same tendency is observed in LHD when the injection angle is changed from the clockwise to counter-clockwise direction. Currently the EC current amplitude is of the same order (few kA) in all of the devices, although the magnetic field structure is different. As discussed later, the toroidal direction of EC current strongly depends on the magnetic ripple structure. Under the condition for toroidal injection scan, the Fisch-Boozer effect may be stronger than the Ohkawa effect. In the injection angle scan with a fixed magnetic field, the electron cyclotron resonance is Doppler-shifted due to finite N_{\parallel} , causing the decrease in electron temperature and/or the change in ripple structure to possibly affect EC current. Study of N_{\parallel} dependence considering the Doppler shift effect is left for future work.

The measured non-inductive current in ECH plasmas is composed of the bootstrap current and the EC current. The exclusion of the bootstrap current is required for accurate estimation of the EC current. One method is to estimate the bootstrap current by an EC beam launch in the direction normal to the magnetic field, where the bootstrap current should be dominant. Another method is to use their different dependencies on the magnetic field direction. The bootstrap current, which is proportional to $\mathbf{B} \times \nabla B$ drift, changes the flow direction when the magnetic field is reversed, while the EC current associated with the B strength does not change its flow direction. Magnetic field reversal experiments were conducted in Heliotron J in order to separate the EC current from the bootstrap current. We confirmed that the global plasma parameters such as stored energy and T_e did not change when reversing the magnetic field direction. Figure 3 shows the density dependence of the estimated bootstrap current and the EC current in Heliotron J. The bootstrap current increases with increasing plasma density, and saturates at $n_e > 1.0 \times 10^{19} \text{ m}^{-3}$. This amplitude of bootstrap current agrees with a neoclassical prediction [17]. The bootstrap current is less than 0.5 kA at low density, which is smaller than the EC current, so that the toroidal current is mainly driven by ECCD.

In Heliotron J, the magnetic field ripple structure at the power deposition position can be changed over a wide range by controlling the current in each coil. As illustrated in Fig. 1, the power deposition can be varied from the ripple top to the ripple bottom mainly by changing the bumpiness component in the field spectrum with a fixed magnetic field strength. The ratio of the magnetic field at the straight section to the magnetic field at the corner section defined by $h = B(\varphi = 0 \text{ deg})/B(\varphi = 45 \text{ deg})$ ranges from 0.81 to 1.23. Figure 4 shows the density dependence of EC current for three field configurations. Here, the contribution of the bootstrap current is eliminated by the field reversal experiment. It can be seen that the maximum EC current of 4.6 kA is attained at the ripple top heating ($h = 1.06$). The EC current flows in the opposite direction at the ripple bottom heating ($h = 0.82$), and its amplitude is as low as one-third of the ripple top heating.

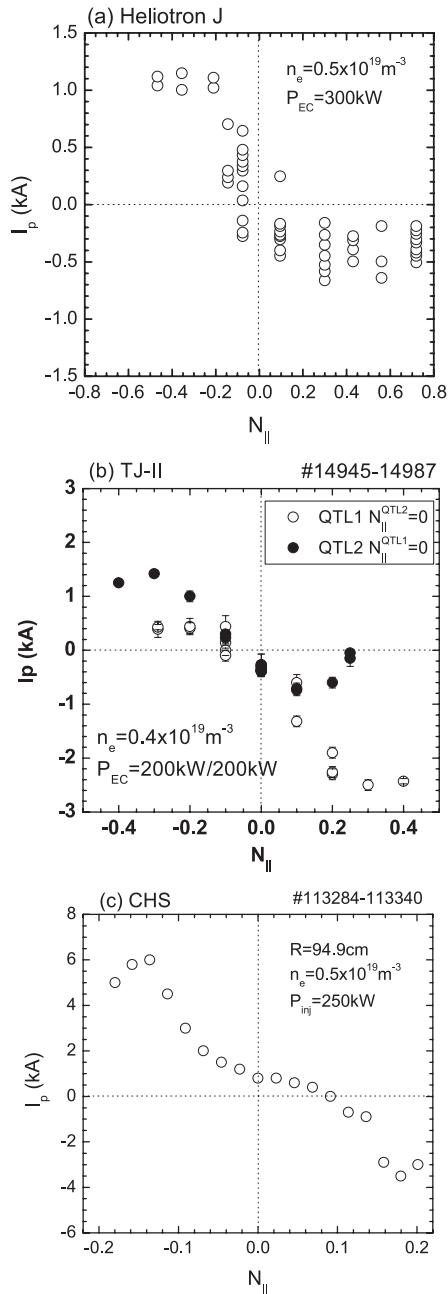


Fig. 2 Dependence of toroidal current on EC injection angle. Magnetic axis in CHS is at 94.9 cm.

One reason for current reversal is that velocity space effects are responsible for the ECCD. The Fisch-Boozer effect considers the perpendicular excursion in the velocity of a group of electrons with positive $v_{||}$. The acceleration of these electrons causes an excess of electrons with counter-clockwise $v_{||}$, resulting in a current in the clockwise toroidal direction. On the other hand, the Ohkawa effect drives current in the direction opposite to the Fisch-Boozer current [18]. The asymmetry in $v_{||}$ is lost due to the bounce in the magnetic ripple, and a deficit in velocity space generates an electrical current in the counter-clockwise toroidal direction. In the high-bumpiness con-

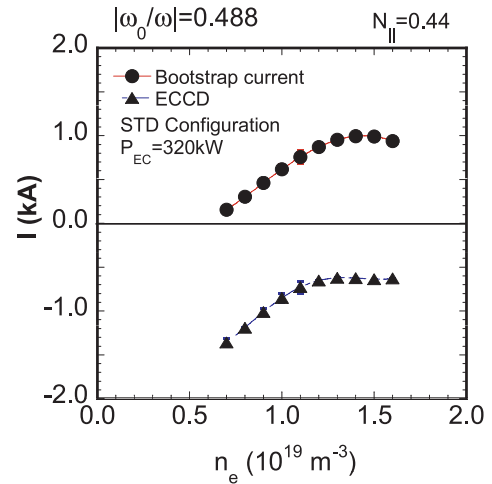


Fig. 3 Separation of bootstrap current and EC current in Heliotron J.

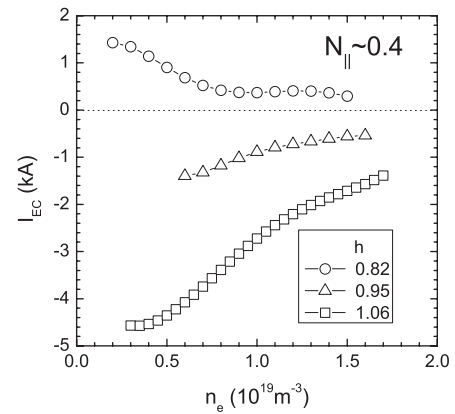


Fig. 4 Density dependence of EC current in Heliotron J. Circles, triangles and squares denote EC current at ripple bottom ($h = 0.82$), flat ($h = 0.95$), and ripple top ($h = 1.06$) heating, respectively.

figuration, the electrons are accelerated in the valley of the ripple, and they tend to become trapped, thus enhancing the Ohkawa effect. These qualitative predictions are consistent with the experimentally measured ECCD direction. The transition from the Fisch-Boozer current drive to the Ohkawa current is also demonstrated in Ref. [5]. In S/H systems, the strength of the Ohkawa effect is comparable to that of the Fisch-Boozer effect, and the ECCD direction is determined by the difference between them.

The experimental results on magnetic field scan in CHS are shown in Fig. 5. The injection angles are $+7$ and -7 deg, and the magnetic axis is fixed; $R_{axis} = 94.9 \text{ cm}$. The Doppler shift of cyclotron resonance is estimated as $(\omega - 2\omega_{ce})/\omega \sim 1\%$ for $T_e = 1 \text{ keV}$ and $N_{||} = 0.16$; thus, the Doppler shift effect is relatively weak. The EC current is largest when the resonance is located at the magnetic axis. The flow direction is consistent with the Fisch-

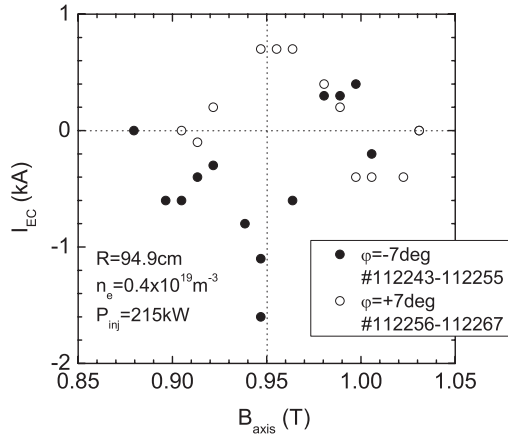


Fig. 5 EC current as function of magnetic field strength in CHS.

Boozer effect. The reduction in current drive efficiency at off-axis ECCD is also observed in Heliotron J. This may be because the electron temperature is decreased and/or the ripple effect is large.

In low-shear devices, even a small amount of current strongly affects rotational transform profile. According to HINT2 code simulation results on a Heliotron J configuration, a localized current of -5 kA changes the central rotational transform from 0.56 to 0.18, generating high magnetic shear at the core region. The rotational transform profile has been measured by an MSE diagnostic in LHD. Figure 6 shows the measurement results for co-ECCD, no ECCD, and ctr-ECCD. Co-ECCD increases the central rotational transform and vice versa. This tendency agrees qualitatively with the direction of the poloidal magnetic field generated by the measured EC current. Quantitative evaluation will be undertaken in a future experiment.

The ratio of driven current to injection power, I_{EC}/P_{EC} , and the figure of merit,

$$\gamma = \frac{n_e I_{EC} R}{P_{EC}}, \quad (1)$$

are conventionally used for estimating of ECCD efficiency. The drawback of these functions is that they have dimensions, and that they do not reflect the T_e dependence. A figure of merit describing dimensionless ECCD efficiency including the T_e dependence is proposed in the following form [3]:

$$\zeta = \frac{e^3 n_e I_{EC} R}{\epsilon_0^2 P_{EC} T_e} = 32.7 \frac{n_e I_{EC} R}{P_{EC} T_e}, \quad (2)$$

Table 2 Electron cyclotron current drive efficiencies in Heliotron J, TJ-II, and CHS.

	Heliotron J	TJ-II	CHS
Maximum I_{EC}	4.6 kA	2 kA	6 kA
$\eta = I_{EC}/P_{EC}$	14 A/kW	10-15 A/kW	35 A/kW
$\gamma = n_e I_{EC} R / P_{EC}$	$\sim 8 \times 10^{16}$ A/Wm ²	$\sim 9 \times 10^{16}$ A/Wm ²	$\sim 16 \times 10^{16}$ A/Wm ²
$\zeta = 32.7 n_{20} I_A R_m / P_W T_{keV}$	~ 0.05	~ 0.03	~ 0.04

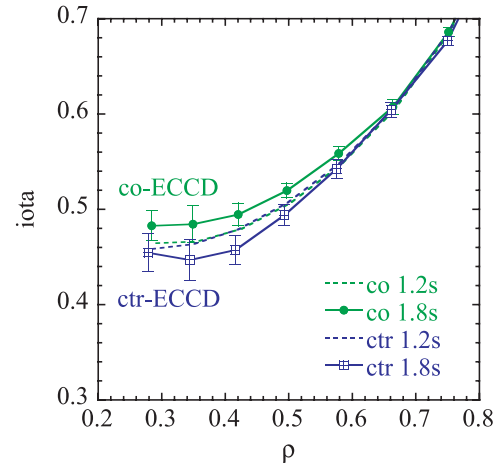


Fig. 6 Measurement of rotational transform by MSE diagnostic in LHD.

where the n_e is in 10^{20}m^{-3} , I_{EC} in A, R in m, P_{EC} in W, and T_e in keV. This dimensionless figure of merit includes important parameters such as n_e and T_e . If ζ changes under the same plasma conditions, it means that ζ reflects the effect of electron thermal velocity and trapping. Table 2 summarizes the ECCD efficiency on Heliotron J, TJ-II, and CHS. No results from LHD are included since such an estimation has not yet been performed because of a short ECH pulse length compared with the current evolution time. It should be noted that these efficiencies are the first typical values ever obtained and not optimized ones. Although the magnetic field structure is different among the devices, the magnitude of the EC current is a few kA in all the devices, and the ECCD efficiency is comparable (within a factor of 2) when the magnetic field ripple ratio, B_{\min}/B_{\max} , ranges from 0.93 to 1.0. This rather low efficiency compared with tokamaks may be due to the strong Ohkawa effect enhanced by the magnetic ripple. The ray tracing calculation code under development will clarify the role of trapped electrons by comparing experimental observations with theory.

Although the ECCD efficiency is not so high, the EC current is comparable to the bootstrap current, meaning that we are able to control the total toroidal current. A zero net current state has been demonstrated in Heliotron J, as shown in Fig. 7. The total current is suppressed below 0.4 kA during the discharge by compensating the bootstrap current of 1.5 kA with ECCD. Such a state has

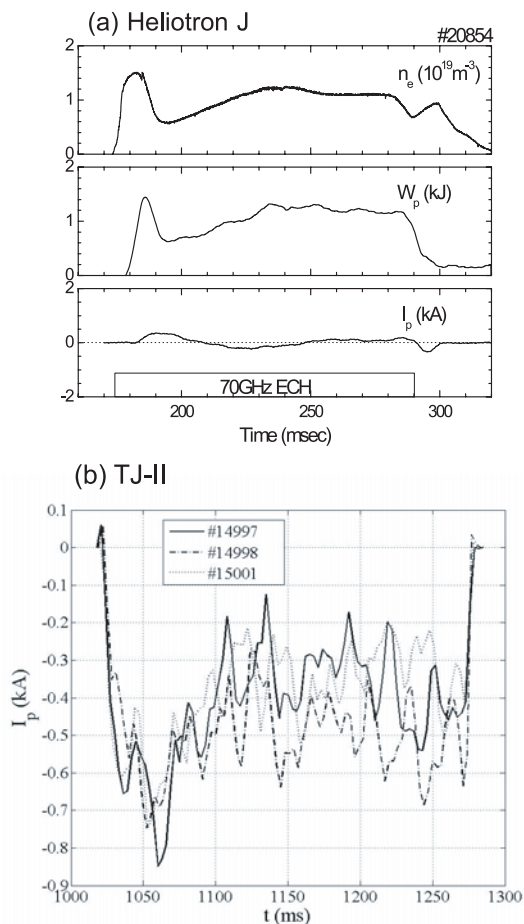


Fig. 7 Demonstration of control of toroidal current: (a) zero toroidal current state in Heliotron J and (b) cancellation of EC current using two unit ECH systems in TJ-II.

also been demonstrated in CHS. In TJ-II, the EC current driven by each launcher is cancelled and the low current of $I_{BS} = -0.5$ kA is maintained. Multi-ECCD systems may be used for extending the current control range.

4. Conclusion

ECCD experiments were performed in Heliotron J, TJ-II, CHS, and LHD. It was found that the driven current is affected by plasma and field parameters such as $N_{||}$, collisionality, resonance position, and magnetic field structure. The injection angle scan experiment indicates that the control ability for EC current is high. The estimated driven current and its efficiency are similar when the magnetic field ripple ratio ranges from 0.93 to 1.0. The

highest current ever observed was 6 kA, and the ECCD efficiency is $\gamma = n_e I_{EC} R / P_{EC} = 8 - 16 \times 10^{16}$ A/Wm², $\zeta = 32.7 n_e I_{EC} R / P_{EC} T_e = 0.03 - 0.05$. In S/H systems, the magnetic ripple structure strongly affects the ECCD. The experiment scanning the magnetic field ripple over a wide range in Heliotron J shows that the direction of EC current is reversed when the power is deposited at the ripple bottom position, indicating that electron trapping is a key factor in determining the EC current.

The EC current is comparable to the bootstrap current, and the ECCD may be favorably used to control the rotational transform profiles. The control of net current has been successfully demonstrated by compensating the bootstrap current with the EC current. Since the bootstrap current profile should be different from the EC current profile, we need to extend the control ability from the viewpoint of the modification of rotational transform, which is closely connected to the suppression of MHD instabilities.

Acknowledgements

The authors are grateful to the Heliotron J, TJ-II, CHS, and LHD staff for conducting the experiments. This study was partly supported by NIFS/NINS under the NIFS Collaborative Research Program (NIFS04KUHL005) and under a project sponsored by the Formation of International Network for Scientific Collaborations.

- [1] Y. Narushima, *J. Plasma Fusion Research* **1**, 004 (2006).
- [2] V. Erckmann and U. Gasparino, *Plasma Phys. Control. Fusion* **36**, 1869 (1994).
- [3] R. Prater, *Phys. Plasmas* **11**, 2349 (2004).
- [4] K. Nagasaki *et al.*, *Nucl. Fusion* **45**, 1608 (2005).
- [5] V. Erckmann *et al.*, *Nucl. Fusion* **43**, 1313 (2003).
- [6] H. Maaßberg *et al.*, *Plasma Phys. Control. Fusion* **47**, 1137-1163 (2005).
- [7] G. Motojima *et al.*, *Nucl. Fusion* **47**, 1045 (2007).
- [8] A. Fernández *et al.*, *Fusion Sci. Technol.* **53**, 254 (2008).
- [9] Y. Yoshimura *et al.*, *J. Korean Phys. Soc.* **49**, S197 (2006).
- [10] Y. Yoshimura *et al.*, *Fusion Sci. Technol.* **53**, 54 (2008).
- [11] T. Notake *et al.*, *Proc. 16th International Stellarator/Heliotron Workshop*, Toki, 2007.
- [12] H. Shidara *et al.*, *Fusion Sci. Technol.* **45**, 41 (2004).
- [13] A. Fernández *et al.*, *Int. J. Infrared and Millimeter Waves* **22**, 649 (2001).
- [14] Y. Yoshimura *et al.*, *J. Phys. Soc. Jpn.* **75**, 114501 (2006).
- [15] T. Shimosuma *et al.*, *Fusion Sci. Technol.* **50**, 403 (2006).
- [16] N. J. Fisch and A. Boozer, *Phys. Rev. Lett.* **45**, 720 (1980).
- [17] G. Motojima *et al.*, *Fusion Sci. Technol.* **51**, 122 (2007).
- [18] T. Ohkawa, *General Atomics Report GA-A13847* (1976).